Hierarchical meso/macro-porous TiO$_2$/graphitic carbon nitride nanofibers with enhanced hydrogen evolution

Xinxin Zou [a,1], Yanling Yang [a,*,1], Huajun Chen [a,b,1], Xiao-Lei Shi [c,d,1], Shaoli Song [e,*], Zhi-Gang Chen [c,d,*]

[a] School of Materials Science and Engineering, Shaanxi Key Laboratory of Green Preparation and Functionalization for Inorganic Materials, Shaanxi University of Science and Technology, Xi'an 710021, PR China
[b] Department of Environment and Chemistry, Luoyang Institute of Science and Technology, Luoyang 471023, PR China
[c] Centre for Future Materials, University of Southern Queensland, Springfield Central, QLD 4300, Australia
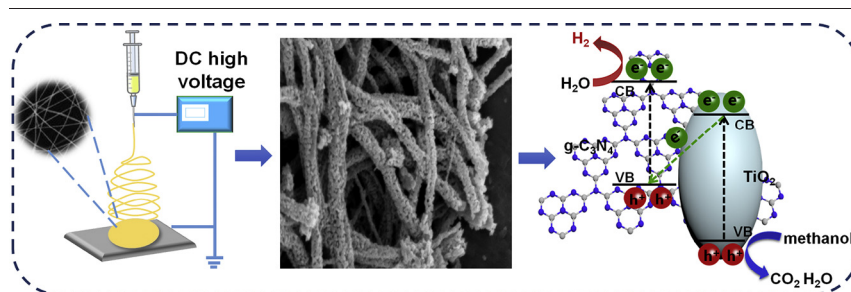[d] School of Mechanical and Mining Engineering, The University of Queensland, QLD 4072, Australia
[e] Nuclear Medicine Department, Fudan University Shanghai Cancer Center, No. 270 Dong'an Road, Xuhui district, Shanghai 200032, China

HIGHLIGHTS

- TiO$_2$/g-C$_3$N$_4$ nanofibers prepared by electrospinning in one step.
- The hierarchical meso/macro-porous structure can be easily obtained by a simple method.
- Hierarchical meso/macro-porous can balance the light-harvesting ability and specific surface area.
- Hierarchical meso/macro-porous create effective transport channel and facilitate molecules spread.

GRAPHICAL ABSTRACT

ARTICLE INFO

ABSTRACT

Constructing a hierarchical structure with tunable pore size is a practical method to improve the capacity of photocatalytic hydrogen production of catalysts. In this work, titanium dioxide/graphitic carbon nitride (TiO$_2$/g-C$_3$N$_4$) nanofibers with hierarchical meso/macro-porous structure are fabricated by combining a one-step electrospinning method and calcination process, in which the hierarchical meso/macro-porous structure is developed by introducing polyvinylpyrrolidone and liquid paraffin into the electrospinning solution. Comprehensive characterizations reveal that the hierarchical meso/macro-porous TiO$_2$/g-C$_3$N$_4$ nanofibers have improved ultraviolet-visible light absorption, the separation efficiency of carriers, and photocatalytic performance. The photocatalytic H$_2$ evolution is up to 1202 μmol g^{-1} in 7 h, which is better than those of corresponding TiO$_2$/g-C$_3$N$_4$ photocatalysts previously reported. This work provides a new strategy to build a hierarchical meso/macro-porous nanofiber and an ideal solution to improve the hydrogen production of TiO$_2$/g-C$_3$N$_4$.

1. Introduction

The renewable energy technologies have been used to tackle the challenges in the global energy shortage. Among various renewable energy technologies, photocatalytic water-splitting for H$_2$ evolution with the potential to realize the conversion and utilization of abundant solar energy has received widespread attention. A variety of efficient photocatalysts, including TiO$_2$ [1], ZnO [2], SnO$_2$ [3], Fe$_2$O$_3$ [4], Cu$_2$O [5], and g-C$_3$N$_4$ [6], have been used for photocatalytic water-splitting for H$_2$ evolution. Among them, TiO$_2$ has been commonly studied because of its competitive advantages, such as excellent chemical stability, non-toxicity, economic effectiveness, and good photocatalytic performance [7]. But the lower efficiency of visible-light absorption and carriers separation limits the

* Corresponding authors.
E-mail addresses: yangyanling@sust.edu.cn (Y. Yang), shaoli-song@163.com (S. Song), zhigang.chen@usq.edu.au (Z.-G. Chen).
[1] The first four authors contributed equally to this work.

applications of single-component TiO_2 photocatalysts. Therefore, searching new-type TiO_2-based photocatalysts with excellent visible-light photocatalytic activity is urgently needed.

So far, the common strategies for suppressing photoinduced carriers recombination and raising the light-absorption capacity of TiO_2 include morphology control [8], element doping [9], heterojunction [10], and cocatalysts [11]. Among these strategies, heterojunction composites have shown their capability for valid harvesting light and guiding the spatial separation/transfer of carriers, thus improving the performance of photocatalytic redox [12]. Recently, the novel visible-light-driven photocatalyst graphitic carbon nitride ($g-C_3N_4$) has been shown to have enhanced activity in the photocatalytic splitting of water [13] and organic pollutants degradation because of its narrow bandgap (approximately 2.7 eV) [14], non-toxicity, low-cost, and high chemical stability [15]. However, the lower photocatalytic performances of single-component $g-C_3N_4$ hinder its practical application.

Considering the stability of TiO_2 and visible-light response ability of $g-C_3N_4$, a heterojunction of $TiO_2/g-C_3N_4$ can effectively enhance the absorption of visible light, prevent the recombination of photoinduced electrons and holes, and meanwhile improve the redox ability. $TiO_2/g-C_3N_4$ heterojunction is usually fabricated by sol-gel and hydrothermal methods [16,17]. These synthetic methods of $TiO_2/g-C_3N_4$ heterojunction are complicated and costly. Thus, it is desirable to develop a facile, low-cost and eco-friendly method to fabricated $TiO_2/g-C_3N_4$ heterojunction. Recently, electrospinning strategy has been shown to be simple and versatile to fabricate single-component, double-component and multi-component fibers with excellent performance because of its advantages, such as controllable preparation craft, short preparation cycle, and a favorable environmental footprint [18,19]. Additionally, meso/macro-porous materials possess many merits. For instance, multiple scattering in pore channels enhance light-harvesting ability of mesoporous materials [20]. A porous structure can also promote the migration of electrons, which has been shown to suppress the carrier recombination [21]. Moreover, the porous structure is beneficial to a large specific surface area that can provide an abundance of reactive sites for the adsorption of reactants [22]. Y.H. Huang and co-workers [23] prepared hierarchically bimodal porous $g-C_3N_4$ nanosheets by a facile method, and the photocatalytic activity was significantly improved. Compared with single-component $g-C_3N_4$, the $TiO_2/g-C_3N_4$ heterojunction has a higher separation efficiency of photogenerated carriers, which is beneficial to the improvement of photocatalytic performance. However, there are few reports about the fabrication of meso/macro-porous $TiO_2/g-C_3N_4$ heterojunction by one-step electrospinning method.

In this work, a facile electrospinning strategy was employed to fabricate $TiO_2/g-C_3N_4$ heterojunction with a hierarchical meso/macro-porous structure. The hierarchical meso/macro-porous $TiO_2/g-C_3N_4$ heterojunction with both the stability of TiO_2 and visible-light response ability of $g-C_3N_4$ shows the enhanced absorption of visible light, the lower recombination of photoinduced electrons and holes, and the higher redox ability. The introduction of a hierarchical meso/macro-porous structure endows $TiO_2/g-C_3N_4$ heterojunction with high light-harvesting ability, short transport distance of photo-excited electron/hole, and high specific surface. Abundant pore channels afford more effective transport path and facilitate the spread of molecules in the reaction process. The performance and mechanism of photocatalytic water-splitting for H_2 evolution of hierarchical meso/macro-porous $TiO_2/g-C_3N_4$ heterojunction were fully investigated. The results indicate that hierarchical meso/macro-porous $TiO_2/g-C_3N_4$ heterojunction show excellent photocatalytic performance, which can be used for water-splitting for H_2 evolution.

2. Experimental

2.1. Chemicals and materials

Analytical grade reagents, including polyvinylpyrrolidone (PVP; Mw = 1,300,000), butyl titanate ($C_{16}H_{36}O_4Ti$), urea ($CO(NH_2)_2$), acetic acid (CH_3COOH), N, N-dimethylformamide (DMF), anhydrous ethanol (C_2H_5OH), methanol (CH_3OH), and liquid paraffin, were bought from Macklin Reagent Co., Ltd., and un-purified for fabricate hierarchical meso/macro-porous $TiO_2/g-C_3N_4$ nanofibers.

2.2. Samples preparation

An electrospinning technique followed by a calcination process was used to fabricate hierarchical meso/macro-porous $TiO_2/g-C_3N_4$ nanofibers. First, DMF, absolute ethanol, and acetic acid were mixed and dissolved to form a solute with volumes of 8 mL, 6.4 mL, and 1.2 mL, respectively. Following this, 0.60 g urea was added to the solution until fully dissolved, and then 1.20 g PVP was added and mixed. After that, the solution was incorporated with 3 mL butyl titanate and stirred for 30 min. Finally, certain doses of liquid paraffin were introduced into the system and stirred for more than 48 h to achieve the precursor solution.

The electrospinning apparatus consisted of a high-voltage power supply (0–30 kV), a micro-injection pump, and a syringe with a capillary tip diameter of 0.6 mm. The electric field was 18 kV, and the distance between the capillary tip and aluminum plate collector is 20 cm. The constant rate of the micro-injection pump is 1.0 mL h^{-1}. After electrospinning, the electrospinning products were collected and calcined in air at 500 °C for 4 h under a heating rate of 5 °C min^{-1}. The samples obtained when the liquid paraffin content is 0 and 0.10 g mL^{-1} are *meso*porous $TiO_2/g-C_3N_4$ nanofibers and hierarchical meso/macro-porous $TiO_2/g-C_3N_4$ nanofibers, respectively.

2.3. Characterization of the photocatalysts

Scanning electron microscopy (SEM, FEI Verios 460, USA) and transmission electron microscopy (TEM, FEI Tecnai G2 F20 S-TWIN, USA) were used to characterize the microstructure of $TiO_2/g-C_3N_4$ nanofibers. The crystalline structures of samples were characterized by X-ray diffraction (XRD, Rigaku D/max2200Pc, Japan). The ultraviolet-visible (UV–Vis) diffuse reflection spectroscopy (DRS) and photoluminescence spectroscopy were tested on Agilent CARY 5000 spectrophotometer and Hitachi F-4500 fluorescence spectrophotometer, respectively. X-ray photoelectron spectra (XPS, AXIS SUPRA, UK) were tested using Mg K radiation (hr = 1253.6 eV), and containment carbon (C 1 s = 284.6 eV) was used to calibrate the binding energy during the test. The specific surface area of the samples was researched by physisorption of N_2 at 77 K using a Micromeritics ASAP2460 instrument. The specific surface area of the samples was related to the linear portion of the Brunauer-Emmett-Teller (BET) plot. Before measurement, the samples were degassed at a vacuum of 300 °C for 6 h to eliminate the components of the prep-adsorbed. The total pore volumes were calculated by the formula of Barrett-Joyner-Halenda (BJH). At room temperature, the photocurrent and electrochemical impedance spectroscopy (EIS) of $TiO_2/g-C_3N_4$ nanofibers was determined on a CHI660D electrochemical workstation. The platinum electrode, saturated calomel electrode (SCE), and $TiO_2/g-C_3N_4$ nanofibers in a standard three-electrode cell were counter electrode, reference electrode, and working electrode, respectively. The electrolyte used was a sodium sulfate solution.

2.4. Photocatalytic hydrogen production

The photocatalytic activity of the as-fabricated hierarchical meso/macro-porous $TiO_2/g-C_3N_4$ nanofibers was appraised by photocatalytic water-splitting for H_2 evolution test under simulated-solar light irradiation. A quartz reactor with a top irradiation and a closed glass gas circulation system was used to conduct the reaction of photocatalytic H_2 production, and the irradiation light source was a 300 W Xenon (Xe) lamp equipped with AM 1.5 filter. Before light irradiation, the suspension containing 50 mg catalyst, 37.5 mL deionized water, and 12.5 mL CH_3OH, was dispersed in an ultrasonic bath for 10 min. In order to

fully remove the oxygen dissolved in the suspension, nitrogen was introduced into the reactor and bubbled for 1 h. CH_3OH is a sacrificial electron donor and react with the photoinduced hole of valance band, which could benefit for the separation of photo-excited carriers. To achieve homogeneous irradiation of the photocatalyst suspension, vigorous agitation was conducted during the entire reaction process. During the reaction of photocatalytic, the reaction solution temperature was stabilized at 6 °C by a flow of cool water. Gas chromatography (CLARUS 580 GC, PerkinElmer) with a thermal conductivity detector and nitrogen carrier gas were used for the online measurement of evolved gas.

3. Results and discussion

Fig. 1a displays a diagrammatic sketch of electrospinning preparation of hierarchical meso/macro-porous $TiO_2/g-C_3N_4$ nanofibers and the influence of the volatilization of PVP and liquid paraffin on the microstructure of hierarchical meso/macro-porous $TiO_2/g-C_3N_4$ nanofibers. Hierarchical meso/macro-porous $TiO_2/g-C_3N_4$ nanofibers were fabricated using PVP and liquid paraffin as a soft template. Fig. 1b plots XRD patterns of mesoporous TiO_2 nanofibers, mesoporous $TiO_2/g-C_3N_4$ nanofibers and hierarchical meso/macro-porous $TiO_2/g-C_3N_4$ nanofibers. As can be seen, mesoporous $TiO_2/g-C_3N_4$ nanofibers and hierarchical meso/macro-porous $TiO_2/g-C_3N_4$ nanofibers contain anatase phases of TiO_2 (JCPDS card No. 21–1272). In the XRD pattern of pure $g-C_3N_4$, characteristic peaks, centered at ~13.1° and 27.4°, correspond to (100) and (002) of $g-C_3N_4$ (JCPDS card No. 87–1526) [24]. Compared with mesoporous TiO_2 nanofibers, a characteristic peak of $g-C_3N_4$ at ~27.4° can be observed in the $TiO_2/g-C_3N_4$ nanofibers, but a characteristic peak at ~13.1° disappears, which should be attributed to the low urea content in the fabrication. These XRD results indicate the hybrids of TiO_2 and $g-C_3N_4$ are successfully fabricated. Due to the low content of urea in the fabrication, the (100) of the $TiO_2/g-C_3N_4$ samples disappeared and the (002) characteristic peak exists. It shows that the hybrid of TiO_2 and $g-C_3N_4$ was successfully fabricated. Fig. 1c-f show the morphologies of the samples. Fig. 1c and e show the typical SEM
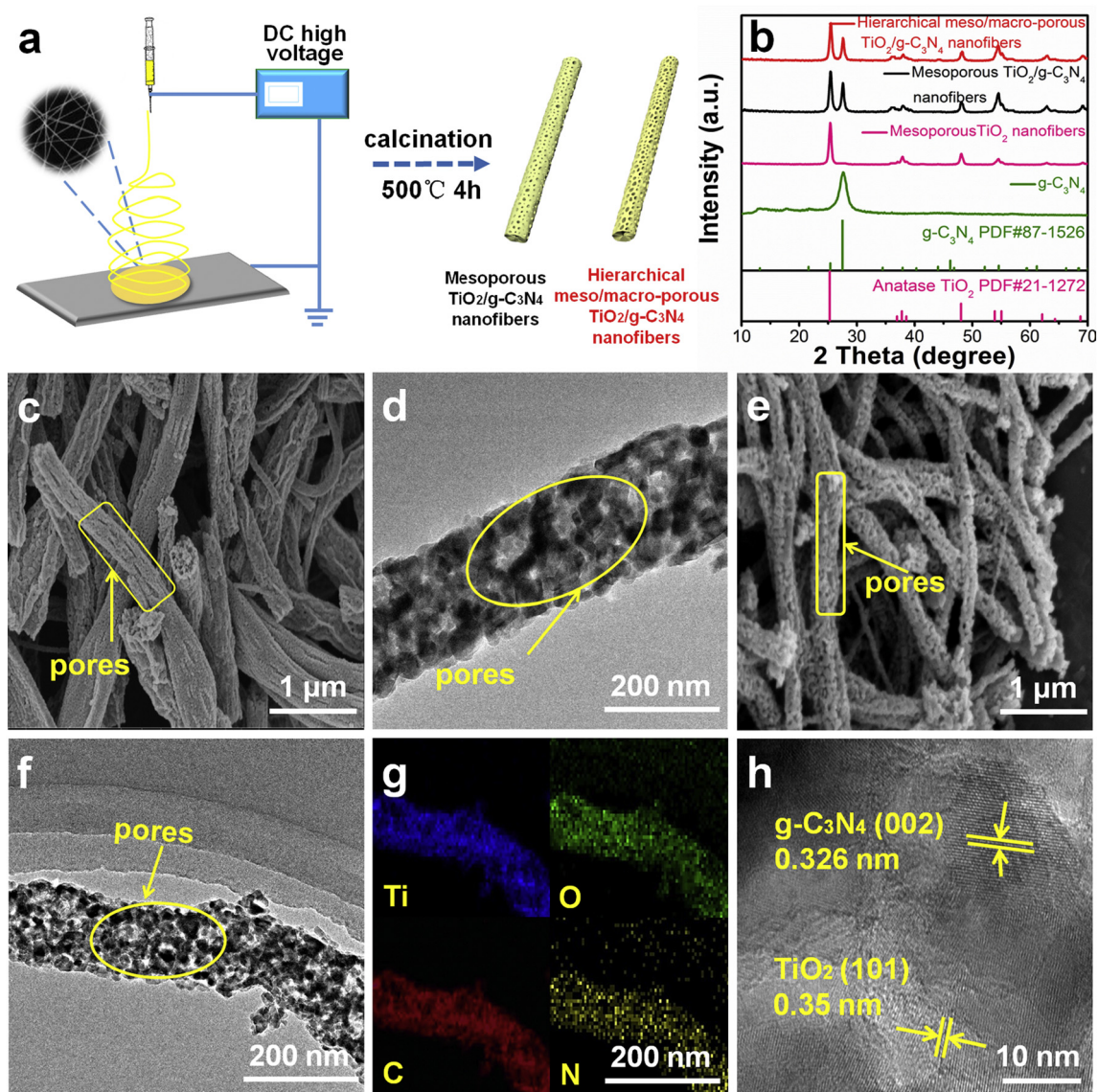

Fig. 1. (a) Sketch map of the electrospinning preparing process and the influence of the volatilization of PVP and liquid paraffin on $TiO_2/g-C_3N_4$ samples. (b) XRD patterns of $g-C_3N_4$, mesoporous TiO_2 nanofibers, mesoporous $TiO_2/g-C_3N_4$ nanofibers and hierarchical meso/macro-porous $TiO_2/g-C_3N_4$ nanofibers. SEM and TEM images of samples: (c, d) mesoporous $TiO_2/g-C_3N_4$ nanofibers; (e, f) hierarchical meso/macro-porous $TiO_2/g-C_3N_4$ nanofibers. (g) Mappings of Ti, O, C and N elements in hierarchical meso/macro-porous $TiO_2/g-C_3N_4$ nanofibers. (h) HRTEM image of hierarchical meso/macro-porous $TiO_2/g-C_3N_4$ nanofibers.

images of mesoporous TiO_2/g-C_3N_4 nanofibers and hierarchical meso/macro-porous TiO_2/g-C_3N_4 nanofibers, and it is obvious that the morphology of nanofibers is uniform. It can be seen that the surface of TiO_2/g-C_3N_4 nanofibers is relatively rough and has a large number of pores (Fig. 1c and e). The PVP evenly distributed in the samples undergoes a thermal decomposition during calcination [25], resulting in the formation of a large number of pores on the surface of mesoporous TiO_2/g-C_3N_4 nanofibers (Fig. 1c). As shown in Fig. 1e, compared with mesoporous TiO_2/g-C_3N_4 nanofibers, the pore size and porosity of hierarchical meso/macro-porous TiO_2/g-C_3N_4 nanofibers are significantly increased. During the drying process, the uniformly distributed liquid paraffin gradually aggregates together in the nanofibers [26], and then the aggregated liquid paraffin quickly volatilizes at high temperatures, leading to an increase in pore size and porosity.

To determine the hierarchical meso/macro-porous structure of as-fabricated TiO_2/g-C_3N_4 nanofibers, TEM was used and the results are shown in Fig. 1d and f. As can be seen, mesoporous TiO_2/g-C_3N_4 nanofibers has a smaller pore size and a lower porosity (Fig. 1d) while the pore size and porosity of hierarchical meso/macro-porous TiO_2/g-C_3N_4 nanofibers have increased significantly (Fig. 1f), indicating that the volatilization of liquid paraffin is beneficial to the increase of pore size in nanofibers. EDX mappings of hierarchical meso/macro-porous TiO_2/g-C_3N_4 nanofibers in Fig. 1g shows that the as-fabricated sample contains the elements of Ti, O, C and N, which confirmed the successful combination of the TiO_2/g-C_3N_4 composite material. Fig. 1h is a high-resolution TEM image of hierarchical meso/macro-porous TiO_2/g-C_3N_4 nanofibers and the observed lattice fringes of 0.326 and 0.35 nm represent the d spacing of (002) for g-C_3N_4 [27] and of (101) for anatase TiO_2 (Fig. 1h). The above results show that the synthetic strategy employed in this research successfully fabricated hierarchical meso/macro-porous TiO_2/g-C_3N_4 nanofibers.

To better understand the structures of TiO_2/g-C_3N_4 nanofibers, the N_2 adsorption-desorption isotherms and distribution curves of the pore size of mesoporous TiO_2/g-C_3N_4 nanofibers and hierarchical meso/macro-porous TiO_2/g-C_3N_4 nanofibers were investigated and their results are presented in Fig. 2a-b. Fig. 2a illustrates that all samples have type IV adsorption-desorption isotherms [24]. The isotherms of hierarchical meso/macro-porous TiO_2/g-C_3N_4 nanofibers (Fig. 2a) demonstrate high absorption when the range of P/P_0 is close to 1.0, indicating that both mesopores and macropores coexist [28], as confirmed by the TEM observation (Fig. 1f). As shown in BET results in Fig. 2a, hierarchical meso/macro-porous TiO_2/g-C_3N_4 nanofibers (55.23 $m^2\,g^{-1}$) has a larger specific surface area than that of mesoporous TiO_2/g-C_3N_4 nanofibers (27.96 $m^2\,g^{-1}$). The hierarchical pores structure significantly increases the utilization of the internal surface of the photocatalyst [20], increases

the specific surface area, which is beneficial to full exposure of active catalytic sites. Fig. 2b plots the pore size distribution of mesoporous TiO_2/g-C_3N_4 nanofibers and hierarchical meso/macro-porous TiO_2/g-C_3N_4 nanofibers. The pore structure in mesoporous TiO_2/g-C_3N_4 nanofibers is mostly mesopores (2–50 nm), while hierarchical meso/macro-porous TiO_2/g-C_3N_4 nanofibers has both mesopores and macropores (>50 nm). Furthermore, the porosity of hierarchical meso/macro-porous TiO_2/g-C_3N_4 nanofibers is significantly increased compared with mesoporous TiO_2/g-C_3N_4 nanofibers. The through-hole structure formed by the interconnection of mesopores and macropores provides more effective transport paths and enhances the spread of molecules in the liquid-phase reaction [29].

XPS spectroscopy was used to characterize the composition and chemical states of elements in hierarchical meso/macro-porous TiO_2/g-C_3N_4 nanofibers. Based on the C 1 s at 284.6 eV, the peaks in XPS results were identified. Fig. 3a shows that the product comprises Ti, O, C, and N elements according to the peaks at the corresponding positions, and peaks of other elements are not detected. The appearance of the N element in the spectra is attributed to the addition of g-C_3N_4 [30], indicating that TiO_2 and g-C_3N_4 are successfully combined. Fig. 3b illustrates the XPS spectrum of Ti 2p in the hybrids. As can be seen, two obvious peaks occur at approximately 458.4 eV (Ti 2 $p_{3/2}$) and 464.1 eV (Ti 2 $p_{1/2}$) of the Ti 2 p spectrum [24], indicating that Ti (Ti^{4+}) exists in a normal state. Fig. 3c shows that the peak of O 1 s at approximately 529.8 eV is related to the Ti—O band in TiO_2 [31], while another peak at approximately 531.0 eV could be marked as O—H band [32]. Fig. 3d indicates that the three peaks of C 1 s at 284.6, 286.1, and 288.4 eV, respectively. The stronger peak intensity of 284.6 eV is mainly due to the coordination of C—C, which included the adventitious hydrocarbon in the instrument of XPS and carbon atoms sp^2-hybridized in g-C_3N_4 [33]. The middle peak is from the species of C-NH_2, and the 288.4 eV peak corresponds to the bond of N-C=N [27]. The two main peaks at 399.7 and 400.1 eV in Fig. 3e belonged to the C-N-H bonding [24] and N-$(C)_3$ [27], respectively. Hierarchical meso/macro-porous TiO_2/g-C_3N_4 nanofibers has lower N 1 s binding energy than that of pure g-C_3N_4 [24], which means that there exists a strong interaction in the TiO_2/g-C_3N_4 interface instead of simple physical mixing [34]. On this basis, we believe that electrons transfer from TiO_2 to g-C_3N_4 in the hybrids.

In order to evaluate optical absorptivity of hierarchical meso/macro-porous TiO_2/g-C_3N_4 nanofibers, DRS was used and the results are shown in Fig. 4a. Compared with TiO_2 nanofibers, the absorption edge of TiO_2/g-C_3N_4 nanofibers has a redshift and the light absorption rate in the visible light region increases, which suggests that the addition of g-C_3N_4 can improve the visible-light absorption capacity, and the improvement of light absorption performance can be conducive to the production of
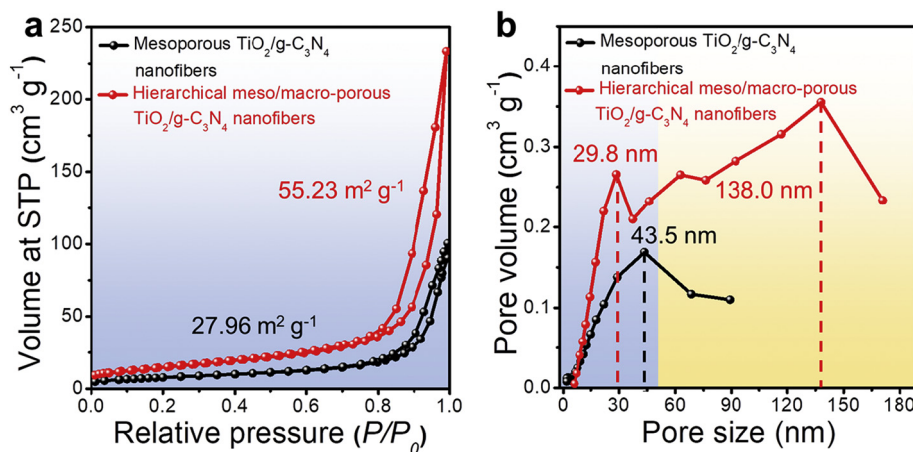

Fig. 2. (a) N_2 adsorption-desorption isotherms and (b) corresponding pore size distributions of mesoporous TiO_2/g-C_3N_4 nanofibers and hierarchical meso/macro-porous TiO_2/g-C_3N_4 nanofibers samples.

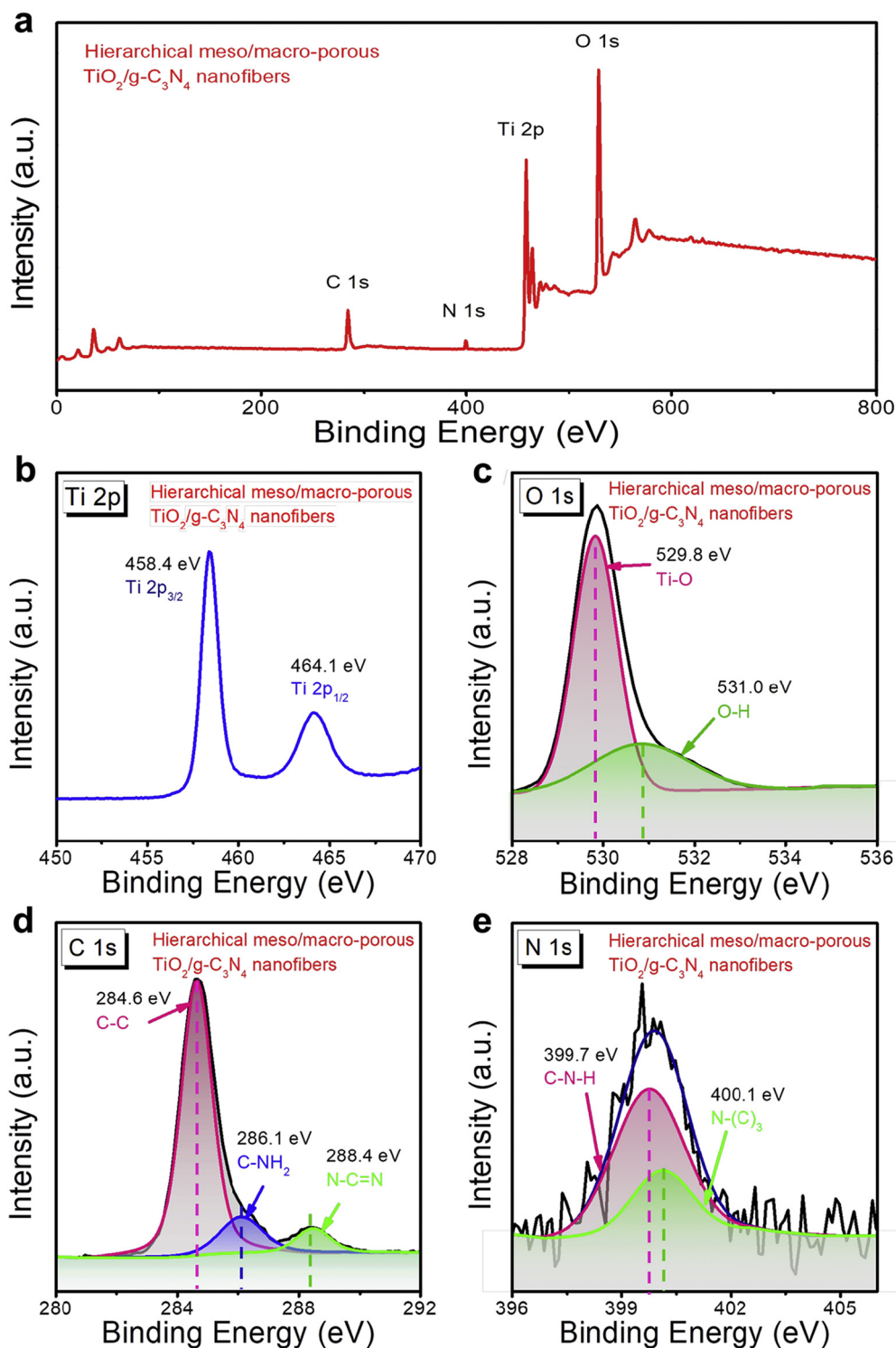**Fig. 3.** XPS spectra of hierarchical meso/macro-porous TiO₂/g-C₃N₄ nanofibers: (a) full spectrum and corresponding spectrum of (b) Ti 2 p, (c) O 1 s, (d) C 1 s, and (e) N 1 s.

more photocatalytic active substances. Furthermore, hierarchical meso/macro-porous TiO₂/g-C₃N₄ nanofiber has stronger light adsorption than mesoporous TiO₂/g-C₃N₄ nanofibers in the range of 200–350 nm. This is due to the introduction of a macro-porous structure that increases the paths of light traveling and raises the ability of light-harvesting [20]. Fig. 4b shows an approximation of the bandgap of mesoporous TiO₂/g-C₃N₄ nanofibers and hierarchical meso/macro-porous TiO₂/g-C₃N₄ nanofibers. The bandgaps of mesoporous TiO₂/g-C₃N₄ nanofibers and

hierarchical meso/macro-porous TiO₂/g-C₃N₄ nanofibers are 3.07 and 3.01 eV. The disparity in the structures cause a subtle difference in the bandgap [26], meaning that the structure of hierarchical meso/macro-porous is favorable to shorten the bandgap. The intensity of the photoluminescence spectra was used to evaluate the recombination rates of photo-excited electron-hole pairs. Fig. 4c shows the photoluminescence emission spectra of mesoporous TiO₂/g-C₃N₄ nanofibers and hierarchical meso/macro-porous TiO₂/g-C₃N₄ nanofibers. The emission intensity
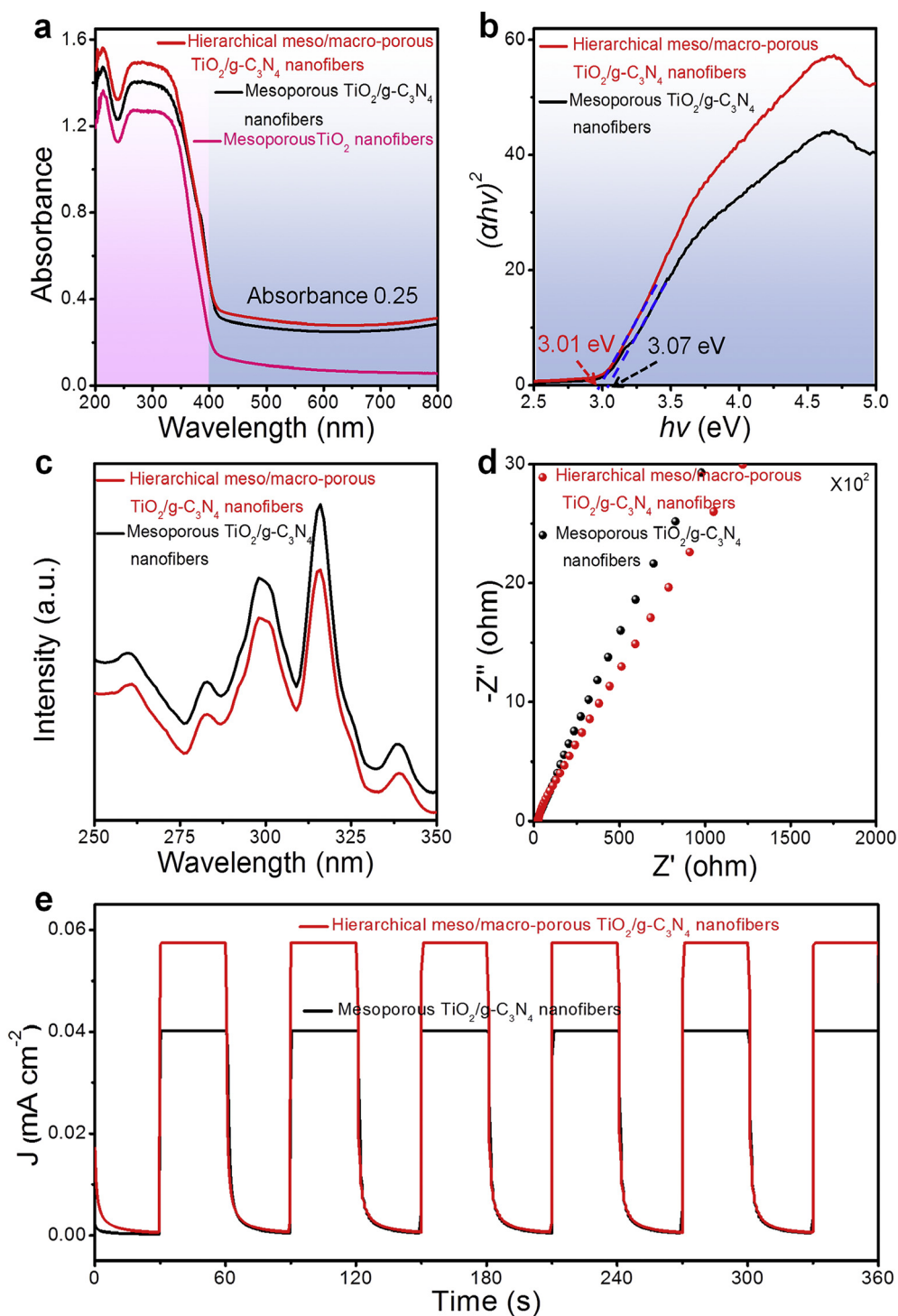
Fig. 4. (a) UV–vis diffuse reflectance spectra of mesoporous TiO_2 nanofibers, mesoporous TiO_2/g-C_3N_4 nanofibers and hierarchical meso/macro-porous TiO_2/g-C_3N_4 nanofibers, (b) bandgap energy, (c) photoluminescence emission spectra, (d) EIS plots and (e) photocurrent under simulated-solar light irradiation of mesoporous TiO_2/g-C_3N_4 nanofibers and hierarchical meso/macro-porous TiO_2/g-C_3N_4 nanofibers.

of hierarchical meso/macro-porous TiO_2/g-C_3N_4 nanofibers is suppressed at 250–350 nm, indicating that lower photo-excited charge recombination efficiency for hierarchical meso/macro-porous $TiO_2/$ g-C_3N_4 nanofibers. The reason for low photo-excited charge recombination efficiency is that the hierarchical meso/macro-porous structure is conducive to the transfer and separation of charges, thereby inhibiting charges recombination [35]. The carrier separation efficiency of $TiO_2/$ g-C_3N_4 nanofibers is analyzed by using EIS. Fig. 4d exhibit the EIS

Nyquist plots of TiO_2/g-C_3N_4 nanofibers. As can be seen, the arc radius of hierarchical meso/macro-porous TiO_2/g-C_3N_4 nanofibers is smaller than mesoporous TiO_2/g-C_3N_4 nanofibers, suggesting that TiO_2/g-C_3N_4 nanofibers with a hierarchical meso/macro-porous structure have lower charge transfer resistance than TiO_2/g-C_3N_4 nanofibers. This result indicates that the pore structure in the hierarchical meso/macro-porous TiO_2/g-C_3N_4 nanofibers is beneficial to promote the separation and migration of charges [36].

The photocurrent measurements directly reflect the generation and transfer of carriers. Moreover, the photocatalytic ability of the catalyst closely depends on the value of the photocurrent [37]. Fig. 4e illustrates the photocurrent of mesoporous TiO_2/g-C_3N_4 nanofibers and hierarchical meso/macro-porous TiO_2/g-C_3N_4 nanofibers under the simulated-solar light irradiation. The photocurrent densities of hierarchical meso/macro-porous TiO_2/g-C_3N_4 nanofibers are higher than that of mesoporous TiO_2/g-C_3N_4 nanofibers, and the highest value for hierarchical meso/macro-porous TiO_2/g-C_3N_4 nanofibers is 0.057 mA cm^{-2}, which improved by 42.5 % compared to that of mesoporous TiO_2/g-C_3N_4 nanofibers (0.04 mA cm^{-2}). The photocurrent measurements suggest that the hierarchical meso/macro-porous structure improves the light absorption ability and plays a vital role in the production of photocurrents. The photocurrent is stable throughout the photoperiod, which indicates that the as-fabricated photocatalyst is stable during photocatalysis.

The photocatalytic performance of TiO_2/g-C_3N_4 nanofibers was evaluated by photocatalytic water-splitting for H_2 evolution under simulated-solar irradiation. Fig. 5a compares the H_2 evolution activity of mesoporous TiO_2 nanofibers, mesoporous TiO_2/g-C_3N_4 nanofibers and hierarchical meso/macro-porous TiO_2/g-C_3N_4 nanofibers. As shown in Fig. 5a, the H_2 evolution amount of mesoporous TiO_2 nanofibers, mesoporous TiO_2/g-C_3N_4 nanofibers and hierarchical meso/macro-porous TiO_2/g-C_3N_4 nanofibers increases simultaneously as a function of time, but H_2 evolution amount of hierarchical meso/macro-porous TiO_2/g-C_3N_4 nanofibers is greater than that of mesoporous TiO_2 nanofibers and mesoporous TiO_2/g-C_3N_4 nanofibers at all times. After 7 h reaction, the H_2 evolution amount of mesoporous TiO_2 nanofibers, mesoporous TiO_2/g-C_3N_4 nanofibers and hierarchical meso/macro-porous TiO_2/g-C_3N_4 nanofibers are 265 μmol g^{-1}, 453 μmol g^{-1} and 1202 μmol g^{-1}, respectively. In Fig. 5a, the H_2 evolution rate of mesoporous TiO_2 nanofibers, mesoporous TiO_2/g-C_3N_4 nanofibers and hierarchical meso/macro-porous TiO_2/g-C_3N_4 nanofibers are 37 μmol h^{-1} g^{-1}, 64 μmol h^{-1} g^{-1} and 171 μmol h^{-1} g^{-1}, respectively. The H_2 evolution rate of hierarchical meso/macro-porous TiO_2/g-C_3N_4 nanofibers is about 4.62 and 2.65 times greater than that of mesoporous TiO_2 nanofibers and mesoporous TiO_2/g-C_3N_4 nanofibers. Fig. 5b displays the amount of photocatalytic H_2 evolution of mesoporous TiO_2 nanofibers, mesoporous TiO_2/g-C_3N_4 nanofibers and hierarchical meso/macro-porous TiO_2/g-C_3N_4 nanofibers under the light above 420 nm irradiation. It can be seen that the H_2 evolution of mesoporous TiO_2/g-C_3N_4 nanofibers and hierarchical meso/macro-porous TiO_2/g-C_3N_4 nanofibers within 7 h are 193 μmol g^{-1} and

Fig. 5. Amount of photocatalytic H_2 evolution of mesoporous TiO_2 nanofibers, mesoporous TiO_2/g-C_3N_4 nanofibers and hierarchical meso/macro-porous TiO_2/g-C_3N_4 nanofibers under simulated-solar light irradiation (a), under under the light above 420 nm irradiation (b). (c) Cyclic stability test of photocatalytic H_2 evolution activity of hierarchical meso/macro-porous TiO_2/g-C_3N_4 nanofibers under simulated-solar light irradiation.
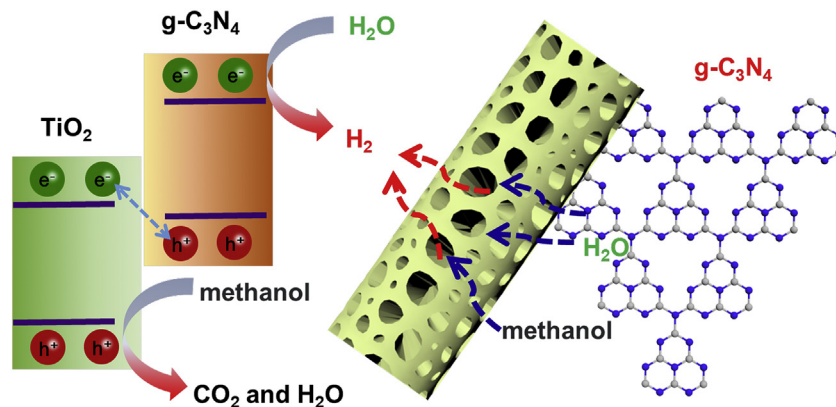
Fig. 6. Photo-excited electrons and holes transfer in composite nanofibers and schematic diagram of molecular diffusion in the photocatalytic process.

327 μmol g^{-1}, respectively. The addition of g-C$_3$N$_4$ broadens the light response range, so that TiO$_2$/g-C$_3$N$_4$ nanofibers have visible light catalytic activity. The higher H$_2$ evolution amount and rate of hierarchical meso/macro-porous TiO$_2$/g-C$_3$N$_4$ nanofibers are ascribed to the improved visible light absorption capacity and photogenerated carrier separation efficiency of the TiO$_2$/g-C$_3$N$_4$ heterojunction. The layered mesoporous/macroporous structure increases the speed of charge transfer and product molecular diffusion [35,38]. Meanwhile, the larger specific surface area provides plentiful reactive sites for H$_2$ evolution [21]. The results of H$_2$ evolution suggest that the through-hole structure formed by the interconnection of mesopores and macropores is beneficial to increase the H$_2$ evolution rate.

The stability of photocatalytic water-splitting for H$_2$ evolution is of importance for photocatalysts in practical application, the photocatalytic stability of hierarchical meso/macro-porous TiO$_2$/g-C$_3$N$_4$ nanofibers is verified by cycling experiments of photocatalytic water-splitting for H$_2$ evolution. As shown in Fig. 5c, the amount of H$_2$ evolution in the first cycle for 4 h is 751 μmol g^{-1}, and the amount of H$_2$ evolution remains to be 691 μmol g^{-1} in the fourth cycle. The H$_2$ evolution activities of hierarchical meso/macro-porous TiO$_2$/g-C$_3$N$_4$ nanofibers is maintained in fourth cycles for 16 h, which indicates good photocatalytic stability of hierarchical meso/macro-porous TiO$_2$/g-C$_3$N$_4$ nanofibers.

The results of photocatalytic water-splitting for H$_2$ evolution of mesoporous TiO$_2$/g-C$_3$N$_4$ nanofibers and hierarchical meso/macro-porous TiO$_2$/g-C$_3$N$_4$ nanofibers indicates that hierarchical meso/macro-porous structure is favored over mesoporous structure in photocatalytic water-splitting for H$_2$ evolution. The higher ascribed to the merits of hierarchical meso/macro-porous structure during photocatalysis. For instance, multiple scattering in hierarchical meso/macro-porous structure enhances light-harvesting ability of mesoporous materials [20]. A hierarchical meso/macro-porous structure can also promote the migration of electrons, which has been shown to suppress the carrier recombination [21]. The hierarchical meso/macroporous structure possesses a large specific surface area that can provide an abundance of reactive sites for the adsorption of reactants [22]. Therefore hierarchical meso/macro-porous structure endows TiO$_2$/g-C$_3$N$_4$ heterojunction with high light-harvesting ability, short transport distance of photo-excited electron/hole, and high specific surface. Furthermore, hierarchical interconnected meso/macro-porous channels afford more effective transport path and facilitate the spread of molecules during photocatalytic process. The interconnected meso/macro-porous channels significantly reduce the transport distance of reactants and products molecules [39]. During the photocatalytic water-splitting for H$_2$ evolution, reactant molecules can easily transport to the reaction sites, and products molecules can also dissociate freely from the reaction sites, which greatly improves the diffusion efficiency of the reactants and products molecules [20].

According to the photocatalytic performance of hierarchical meso/macro-porous TiO$_2$/g-C$_3$N$_4$ nanofibers, a mechanism of photocatalytic water-splitting for H$_2$ evolution is proposed in Fig. 6. Under the irradiation of simulated-solar light, hierarchical *meso*/macro-porous TiO$_2$/g-C$_3$N$_4$ nanofibers generate photo-excited electron-hole pairs. The valence band (VB) and conduction band (CB) potential of TiO$_2$ are 3.1 eV and − 0.1 eV [1], respectively. The VB and CB potential of g-C$_3$N$_4$ are 1.56 eV and − 1.10 eV [32], respectively. The CB potential of TiO$_2$ is more lower than VB potential of g-C$_3$N$_4$, photo-excited electron (e$^-$) will transfers from the CB of TiO$_2$ to the VB of g-C$_3$N$_4$ [24]. Therefore, photo-excited electron and hole will accumulate in the CB of g-C$_3$N$_4$ and the VB of TiO$_2$, respectively. The transfer of photon-excited electron/hole in hierarchical meso/macro-porous TiO$_2$/g-C$_3$N$_4$ nanofibers complies with *Z*-scheme mechanisms [1], which facilitates the separation of photon-excited electron/hole in hierarchical meso/macro-porous TiO$_2$/g-C$_3$N$_4$ nanofibers and in turn extends the life of photon-excited electron/hole [40]. Due to the CB potential of g-C$_3$N$_4$ is lower than the standard reduction potential of H/H$_2$ (0.33 eV), photon-excited electron in the CB of g-C$_3$N$_4$ are captured by H$_2$O to generate H$_2$ molecule in the process of photocatalytic water-splitting for H$_2$ evolution [41].

4. Conclusion

Combining the electrospinning technology and calcination process, TiO$_2$/g-C$_3$N$_4$ nanofibers with hierarchical meso/macro-porous structure have been prepared by adding PVP and liquid paraffin. The measured results of DRS, PL emission spectra, and photocurrent density indicate that a hierarchical meso/macro-porous structure is beneficial to improving the efficiency of light harvesting and carrier separation. The photocatalytic water-splitting for H$_2$ evolution rate of hierarchical meso/macro-porous TiO$_2$/g-C$_3$N$_4$ nanofibers is 171 μmol h^{-1} g^{-1}, which is 2.65 times of mesoporous TiO$_2$/g-C$_3$N$_4$ nanofibers. As-fabricated hierarchical meso/macro-porous structure can increase the migration rate of carrier and the diffusion rate of product molecules, while supplying a large specific surface area and plentiful reactive sites. Our study provides a new strategy to fabricate hierarchical meso/macro-porous TiO$_2$/g-C$_3$N$_4$ nanofibers and a new approach to enhance the catalytic activity of photocatalysts.

Author contributions

All authors have given approval to the final version of the manuscript.

CRediT authorship contribution statement

Xinxin Zou: Investigation, Data curation, Writing - original draft. **Yanling Yang:** Conceptualization, Methodology, Writing - review & editing. **Huajun Chen:** Conceptualization, Data curation, Methodology. **Xiao-Lei Shi:** Investigation, Data curation, Writing - review & editing. **Shaoli Song:** Investigation. **Zhi-Gang Chen:** Conceptualization, Methodology, Visualization, Writing - review & editing.

Declaration of Competing Interest

The authors declare no competing financial interests.

Acknowledgments

References

[1] H.J. Chen, Y.L. Yang, M. Hong, J.G. Chen, G.Q. Suo, X.J. Hou, L. Feng, Z.-G. Chen, Separable and recyclable meso-carbon@TiO$_2$/carbon fiber composites for visible-light photocatalysis and photoelectrocatalysis, Sustain. Mater. Technol. 21 (2019), e00105, .

[2] M.A. Hernández-Carrillo, R. Torres-Ricárdez, M.F. García-Mendoza, E. Ramírez-Morales, L. Rojas-Blanco, L.L. Díaz-Flores, G.E. Sepúlveda-Palacios, F. Paraguay-Delgado, G. Pérez-Hernández, Eu-modified ZnO nanoparticles for applications in photocatalysis, Catal. Today 349 (2020) 191–197.

[3] L. Zhang, R. Tong, S.E. Shirsath, Y. Yang, G. Dong, The crystalline/amorphous stacking structure of SnO$_2$ microspheres for the excellent NO photocatalytic performance, J. Mater. Chem. A (2021) https://doi.org/10.1039/D0TA12101K.

[4] M.M. Ding, W. Chen, H. Xu, Z. Zen, T. Lin, K. Hu, C.H. Lu, Z.L. Xie, Novel alpha-Fe$_2$O$_3$/MXene nanocomposite as heterogeneous activator of peroxymonosulfate for the degradation of salicylic acid, J. Hazard. Mater. 382 (2020) 121064.

[5] D. Chen, Z.F. Liu, Z.G. Guo, W.G. Yan, M.N. Ruan, Decorating Cu$_2$O photocathode with noble-metal-free Al and NiS cocatalysts for efficient photoelectrochemical water splitting by light harvesting management and charge separation design, Chem. Eng. J. 381 (2020) 122655.

[6] K. Wang, Y. Li, J. Li, G.K. Zhang, Boosting interfacial charge separation of Ba$_5$Nb$_4$O$_{15}$/g-C$_3$N$_4$ photocatalysts by 2D/2D nanojunction towards efficient visible-light driven H$_2$ generation, Appl. Catal. B-Environ. 263 (2020) 117730.

[7] Y.L. Yang, H.J. Chen, X.X. Zou, X.-L. Shi, W.-D. Liu, L. Feng, G.Q. Suo, X.J. Hou, X.H. Ye, L. Zhang, C.H. Sun, H.S. Li, C.Q. Wang, Z.-G. Chen, Flexible carbon-fiber/semimetal Bi nanosheet arrays as separable and recyclable plasmonic photocatalysts and photoelectrocatalysts, ACS Appl. Mater. Interfaces 12 (2020) 24845–24854.

[8] X.X. Zou, Y.L. Yang, H.J. Chen, X.L. Shi, G.Q. Suo, X.H. Ye, L. Zhang, X.J. Hou, L. Feng, Z.-G. Chen, Tuning wall thickness of TiO$_2$ microtubes for an enhanced photocatalytic activity with thickness-dependent charge separation efficiency, J. Colloid Interface Sci. 579 (2020) 463–469.

[9] Z. Barbieriková, E. Plížingrová, M. Motlochová, P. Bezdička, J. Boháček, D. Dvoranová, M. Mazúr, J. Kupčík, J. Jirkovský, J. Šubrt, J. Krýsa, V. Brezová, N-doped titanium dioxide nanosheets: preparation, characterization and UV/visible-light activity, Appl. Catal. B-Environ. 232 (2018) 397–408.

[10] C.J. Wang, Y.L. Zhao, H. Xu, Y.F. Li, Y.C. Wei, J. Liu, Z. Zhao, Efficient Z-scheme photocatalysts of ultrathin g-C$_3$N$_4$-wrapped Au/TiO$_2$-nanocrystals for enhanced visible-light-driven conversion of CO$_2$ with H$_2$O, Appl. Catal. B-Environ. 263 (2020) 118314.

[11] J.X. Xu, Q.J. Ji, X.M. Yan, C. Wang, L. Wang, Ni(acac)$_2$/Mo-MOF-derived difunctional MoNi@MoO$_2$ cocatalyst to enhance the photocatalytic H$_2$ evolution activity of g-C$_3$N$_4$, Appl. Catal. B-Environ. 268 (2020) 118739.

[12] L. Liu, L. Ding, Y.G. Liu, W.J. An, S.L. Lin, Y.H. Liang, W.Q. Cui, A stable Ag$_3$PO$_4$@PANI core@shell hybrid: enrichment photocatalytic degradation with π-π conjugation, Appl. Catal. B-Environ. 201 (2017) 92–104.

[13] H.N. Che, G.B. Che, P.J. Zhou, C. Liu, H.J. Dong, C.X. Li, N. Song, C.M. Li, Nitrogen doped carbon ribbons modified g-C$_3$N$_4$ for markedly enhanced photocatalytic H$_2$-production in visible to near-infrared region, Chem. Eng. J. 382 (2020) 122870.

[14] Y.X. Yan, H. Yang, Z. Yi, R.S. Li, T. Xian, Design of ternary CaTiO$_3$/g-C$_3$N$_4$/AgBr Z-scheme heterostructured photocatalysts and their application for dye photodegradation, Solid State Sci. 100 (2020) 106102.

[15] J. Jia, W.J. Sun, Q.Q. Zhang, X.Z. Zhang, X.Y. Hu, E.Z. Liu, J. Fan, Inter-plane heterojunctions within 2D/2D FeSe$_2$/g-C$_3$N$_4$ nanosheet semiconductors for photocatalytic hydrogen generation, Appl. Catal. B-Environ. 261 (2020) 118249.

[16] Z. Lu, L. Zeng, W.L. Song, Z.Y. Qin, D.W. Zeng, C.S. Xie, In situ synthesis of C-TiO$_2$/g-C$_3$N$_4$ heterojunction nanocomposite as highly visible light active photocatalyst originated from effective interfacial charge transfer, Appl. Catal. B-Environ. 202 (2017) 489–499.

[17] J. Wang, G.H. Wang, X. Wang, Y. Wu, Y.R. Su, H. Tang, 3D/2D direct Z-scheme heterojunctions of hierarchical TiO$_2$ microflowers/g-C$_3$N$_4$ nanosheets with enhanced charge carrier separation for photocatalytic H$_2$ evolution, Carbon 149 (2019) 618–626.

[18] D. Li, J.T. McCann, Y. Xia, M. Marquez, Electrospinning: a simple and versatile technique for producing ceramic nanofibers and nanotubes, J. Am. Ceram. Soc. 89 (2006) 1861–1869.

[19] N. Bhardwaj, S.C. Kundu, Electrospinning: a fascinating fiber fabrication technique, Biotechnol. Adv. 28 (2010) 325–347.

[20] X. Li, J.G. Yu, M. Jaroniec, Hierarchical photocatalysts, Chem. Soc. Rev. 45 (2016) 2603–2636.

[21] N. Guo, Y. Zeng, H.Y. Li, X.J. Xu, H.W. Yu, X.R. Han, Novel mesoporous TiO$_2$@g-C$_3$N$_4$ hollow core@shell heterojunction with enhanced photocatalytic activity for water treatment and H$_2$ production under simulated sunlight, J. Hazard. Mater. 353 (2018) 80–88.

[22] W. Tao, M.K. Wang, R. Ali, S. Nie, Q.L. Zeng, R.Q. Yang, W.-M. Lau, L. He, H. Tang, X. Jian, Multi-layered porous hierarchical TiO$_2$/g-C$_3$N$_4$ hybrid coating for enhanced visible light photocatalysis, Appl. Surf. Sci. 495 (2019) 143435.

[23] P. Hu, C.J. Chen, R. Zeng, J.W. Xiang, Y. Huang, D.F. Hou, Q. Li, Y.H. Huang, Facile synthesis of bimodal porous graphitic carbon nitride Nanosheets as efficient Photocatalysts for hydrogen evolution, Nano Energy 50 (2018) 376–382.

[24] Q. Tang, X.F. Meng, Z.Y. Wang, J.W. Zhou, H. Tang, One-step electrospinning synthesis of TiO$_2$/g-C$_3$N$_4$ nanofibers with enhanced photocatalytic properties, Appl. Surf. Sci. 430 (2018) 253–262.

[25] Y.K. Du, P. Yang, Z.G. Mou, N.P. Hua, L. Jiang, Thermal decomposition behaviors of PVP coated on platinum nanoparticles, J. Appl. Polym. Sci. 99 (2010) 254–262.

[26] T. Wang, J.X. Wei, H.M. Shi, M. Zhou, Y. Zhang, Q. Chen, Z.M. Zhang, Preparation of electrospun Ag/TiO$_2$ nanotubes with enhanced photocatalytic activity based on water/oil phase separation, Phys. E. 86 (2017) 103–110.

[27] H. Wei, W.A. McMaster, J.Z.Y. Tan, L. Cao, D. Chen, R.A. Caruso, Mesoporous TiO$_2$/g-C$_3$N$_4$ microspheres with enhanced visible-light photocatalytic activity, J. Phys. Chem. C 121 (2017) 22114–22122.

[28] F. Dong, Z.W. Zhao, T. Xiong, Z.L. Ni, W.D. Zhang, Y.J. Sun, W.-K. Ho, In situ construction of g-C$_3$N$_4$/g-C$_3$N$_4$ metal-free heterojunction for enhanced visible-light photocatalysis, ACS Appl. Mater. Interfaces 5 (2013) 11392–11401.

[29] H.X. Zhao, S. Cui, L. Yang, G.D. Li, N. Li, X.T. Li, Synthesis of hierarchically meso-macroporous TiO$_2$/CdS heterojunction photocatalysts with excellent visible-light photocatalytic activity, J. Colloid Interface Sci. 512 (2018) 47–54.

[30] Y.W. Zhang, J.S. Xu, J. Mei, S. Sarina, Z.Y. Wu, T. Liao, C. Yan, Z.Q. Sun, Strongly interfacial-coupled 2D-2D TiO$_2$/g-C$_3$N$_4$ heterostructure for enhanced visible-light induced synthesis and conversion, J. Hazard. Mater. 394 (2020) 122529.

[31] Y.C. Nie, F. Yu, L.C. Wang, Q.J. Xing, X. Liu, Y. Pei, J.P. Zou, W.L. Dai, Y. Li, S.L. Suib, Photocatalytic degradation of organic pollutants coupled with simultaneous photocatalytic H$_2$ evolution over graphene quantum dots/Mn-N-TiO$_2$/g-C$_3$N$_4$ composite catalysts: performance and mechanism, Appl. Catal. B-Environ. 227 (2018) 312–321.

[32] G.D. Shen, Y.P. Pu, Y.F. Cui, P.P. Jing, Easy synthesis of TiO$_2$/g-C$_3$N$_4$ heterostructure photocatalyst with large surface area and excellent photocatalytic activity, Ceram. Int. 43 (2017) S664–S670.

[33] L.F. Cui, X. Ding, Y.G. Wang, H.C. Shi, L.H. Huang, Y.H. Zuo, S.F. Kang, Facile preparation of Z-scheme WO$_3$/g-C$_3$N$_4$ composite photocatalyst with enhanced photocatalytic performance under visible light, Appl. Surf. Sci. 391 (2017) 202–210.

[34] J.H. Qiu, Y. Feng, X.F. Zhang, X.G. Zhang, M.M. Jia, J.F. Yao, Facile stir-dried preparation of g-C$_3$N$_4$/TiO$_2$ homogeneous composites with enhanced photocatalytic activity, RSC Adv. 7 (2017) 10668–10674.

[35] W. Li, Q. Ma, X. Wang, X.S. Chu, F. Wang, X.C. Wang, C.Y. Wang, Enhanced photoresponse and fast charge transfer: three-dimensional macroporous g-C$_3$N$_4$/GO-TiO$_2$ nanostructure for hydrogen evolution, J. Mater. Chem. A 8 (2020) 19533–19543.

[36] R.V. Nair, P.K. Gayathri, V.S. Gummaluri, C. Vijayan, Optimization of macropore evolution towards high photocatalytic activity enhancement in meso/macro porous anatase TiO$_2$, Mater. Res. Express 4 (2017), 016201, .

[37] J.J. Huo, Y.L. Chen, Y. Liu, J.J. Guo, L. Lu, W.X. Li, Y. Wang, H. Liu, Bifunctional iron nickel phosphide nanocatalysts supported on porous carbon for highly efficient overall water splitting, Sustain. Mater. Technol. 22 (2019), e00117, .

[38] S. Pany, K.M. Parida, Sulfate-anchored hierarchical meso–macroporous N-doped TiO$_2$: a novel photocatalyst for visible light H$_2$ evolution, ACS Sustain. Chem. Eng. 2 (2014) 1429–1438.

[39] J. Du, X.Y. Lai, N.L. Yang, J. Zhai, D. Kisailus, F.B. Su, D. Wang, L. Jiang, Hierarchically ordered macro-mesoporous TiO$_2$-graphene composite films: improved mass transfer, reduced charge recombination, and their enhanced photocatalytic activities, ACS Nano 5 (2010) 590–596.

[40] J. Li, M. Zhang, X. Li, Q.Y. Li, J.J. Yang, Effect of the calcination temperature on the visible light photocatalytic activity of direct contact Z-scheme g-C$_3$N$_4$ -TiO$_2$ heterojunction, Appl. Catal. B-Environ. 212 (2017) 106–114.

[41] P. Zhou, J.G. Yu, M. Jaroniec, All-solid-state Z-scheme photocatalytic systems, Adv. Mater. 26 (2014) 4920–4935.